Published in final edited form as:
Cytometry A. 2016 April ; 89(4): 391–397. doi:10.1002/cyto.a.22794.

High-Throughput Linear Optical Stretcher for Mechanical Characterization of Blood Cells

Kevin B. Roth[1], **Keith B. Neeves**[1,2], **Jeff Squier**[3], **David W. M. Marr**[1]

[1]Chemical and Biological Engineering Department, Colorado School of Mines, Golden, Colorado 80401

[2]Department of Pediatrics, University of Colorado, Denver, Colorado 80045

[3]Department of Physics, Colorado School of Mines, Golden, Colorado 80401

Abstract

This study describes a linear optical stretcher as a high-throughput mechanical property cytometer. Custom, inexpensive, and scalable optics image a linear diode bar source into a microfluidic channel, where cells are hydrodynamically focused into the optical stretcher. Upon entering the stretching region, antipodal optical forces generated by the refraction of tightly focused laser light at the cell membrane deform each cell in flow. Each cell relaxes as it flows out of the trap and is compared to the stretched state to determine deformation. The deformation response of untreated red blood cells and neutrophils were compared to chemically treated cells. Statistically significant differences were observed between normal, diamide-treated, and glutaraldehyde-treated red blood cells, as well as between normal and cytochalasin D-treated neutrophils. Based on the behavior of the pure, untreated populations of red cells and neutrophils, a mixed population of these cells was tested and the discrete populations were identified by deformability.

Keywords

Optical stretcher; optical trap; linear diode bar laser; cell mechanical properties; microfluidics; cell differentiation; deformability cytometry

Introduction

Cell mechanical properties are a label-free biomarker indicative of cell health (1–3); for example, in cases such as malaria (1–4), sickle cell anemia (5), and sepsis (6), cells stiffen with onset of disease. Also, in breast (7,8) and oral (9) cancers, changes in deformability are sufficient to differentiate between cells of varying metastatic potential. Cell mechanics may also be used to assess drug efficacy (1) because various anti-cancer drugs including cytochalasins, vinca alkaloids, and taxanes disrupt the cytoskeleton, inhibiting proliferation by disrupting the cell cycle (10–12) and altering cell mechanics (13,14). In the context

Correspondence to: David W. M. Marr, Chemical and Biological Engineering Department, Colorado School of Mines, Golden, CO 80401, USA. dmarr@mines.edu.

Additional Supporting Information may be found in the online version of this article.

of personalized medicine, the effectiveness of chemotherapeutic agents could be evaluated based on their ability to alter cancer cell mechanics on a per-patient basis (12). However, significant differences exist not only with separate patients but, due to the heterogeneity of tumor tissue and cell response, with individual cells as well. Motivated by this, single cell mechanical properties have been measured by micropipette aspiration (15,16), atomic force microscopy (8,17), and optical tweezing (18,19). These methods, however, employ static testing conditions with low measurement throughput and restricted sample sizes of ~100 cells (20). Because of the inherent heterogeneity of biological samples (21), populations on the order of 10^3–10^4, similar to those generated by techniques such as fluorescence-activated cell sorting (FACS) (22,23), are required to make confident diagnoses based on deformability as a clinical biomarker.

Deforming cells in flow similar to traditional cytometry techniques could increase throughput. One approach is the microfluidic cell deformability cytometer which are inexpensive to prototype, use small sample volumes (nanoliters), and employ laminar flow characteristics (24) allowing for predictable and controllable flow. For example, physical constrictions (25–28) or inertial focusing flow (29–31) have been used to create contact or shear forces (> 1 nN (30)) capable of significantly deforming flowing cells. Large strains (>10% deformation) however, can damage cells and should be avoided when cell isolation and viability post-analysis are of interest. Lower strain (<10% deformation) methods including optical stretchers (7,32) can apply non-destructive, non-contact forces sufficient to differentiate cell states (9,33,34). Optical stretching relies on the changing momentum of laser light by refraction at the surface of a soft dielectric object, generating non-contact optical forces (35). In specific laser configurations (36,37) and when operated at powers that minimize heating from optical absorption (38,39), these forces can deform trapped cells. In the case of a linear optical trap, antipodal stretching forces generated parallel to the trap long axis act to elongate the cell (37), while the relative deforming influence of the hydrodynamic forces remains low (40). By applying optical forces independent of flow forces cell viscoelastic behavior has been accurately quantified via a mechanical model (41). Such techniques can maintain flow velocities capable of deforming 10^3–10^4 cells in 10–20 min while employing geometries very similar to current light-scattering and fluorescence-based imaging cytometers. Because of this and the small perturbations associated with linear optical stretching, direct incorporation of mechanical properties as an additional biomarker within imaging flow cytometers utilizing light and fluorescence-based detection is quite feasible.

Here, we use linear optical stretchers described previously (41,42) to stretch cells continuously in flow. To avoid changes in laser intensity and beam profile due to the linear emitter geometry (43–45), custom optics (37) were used to focus the stretcher at the optimal numerical aperture (NA) with efficient 1:1 imaging of the source (46). In this system, imaging optics are decoupled from the stretching optics.

To test the potential of this system as a high-throughput deformation cytometer, we measured the deformation of normal and chemically treated cells. First, normal human red blood cells (RBCs) were compared to those treated with diamide and glutaraldehyde and the results showed statistically significant increases in stiffness in subsequent populations. As a model for leukemic cells, we isolated and measured the response of normal neutrophils and those treated with cytochalasin D, an actin-disrupting drug. In this, we observed a statistically significant increase in aspect ratio in the treated cell population. Finally, two distinct populations of cells were observed in a mixture of untreated RBCs and neutrophils and differentiated based on aspect ratio.

Materials and Methods

Optical Assembly

Figure 1 shows the optical assembly that was previously described in Ref. 46. A 0.54 NA aspheric lens (A230-C, Thor-Labs, Newton, NJ) first collimates the output from a 1064 nm, 8 W, $1 \times 100\ \mu m^2$ linear diode bar laser (Lumics GmbH, Germany). The linear geometry of the source results in the collimated output extending along the long axis of the bar. A pair of cylindrical lenses (LJ1567RM, ThorLabs, Newton, NJ) forms a telescope to correct for this extension. A second aspheric lens then refocuses the laser after reflection by a dielectric mirror (BB1-E03, ThorLabs, Newton, NJ), forming a 1:1 image of the source through the polydimethylsiloxane (PDMS) layer of a microfluidic device. The near-infrared wavelength of the laser minimizes absorption by biological samples, preventing optical damage (38,39). The laser imaging optics described in Figure 1 are used to create the linear stretcher, shown as a green line in the schematic and images in Figure 2. Sample imaging is achieved through an independent optical train. Light from a 200 W source (Prior Scientific Inc., Rockland, MA) passes through an aperture, condensing lens, dichroic mirror, and aspheric lens to illuminate the sample plane. A ×40 microscope objective (Zeiss LD Achroplan 40×/0,60, Jena, Germany) forms an image (0.1395 μm/pixel) on a Phantom v341 high-speed camera (Vision Research, Wayne, NJ) after a shortpass filter (FES0900 ThorLabs, Newton, NJ) and focusing lens.

Cell Preparation

Blood was obtained according to the Declaration of Helsinki and under either Colorado Multiple Institutional Review Board or the University of Colorado, Boulder Institutional Review Board approved protocols for RBC or neutrophil experiments, respectively. Blood used in the RBC experiments was acquired via finger-poke with a contact-activated safety lancet (BD, Franklin Lakes, NJ). Twenty microliters of blood was then collected via micropipette and suspended in 150 mOsm phosphate buffered saline (PBS) solution with 0.1% wt/vol bovine serum albumin (BSA, Sigma, St. Louis, MO) to prevent non-specific cell interactions and 1.0% wt/vol sodium citrate (Sigma) as anticoagulant. RBCs were swollen to make image processing more uniform. Untreated RBC experiments were performed without the addition of any additional chemicals to the blood suspension. Chemically treated RBCs were suspended in either 3.8 mM diamide (Sigma) or 0.05% vol/vol glutaraldehyde (Sigma) solutions. Regardless of treatment, cells were incubated at room temperature (~25°C) for 20 min before three washes in PBS buffer at 300*g* for 5 min. Cells were suspended in 500 μL of PBS buffer (~2×10^5 cells/μL) for cytometry experiments.

Neutrophils were isolated using a previously described isolation protocol with minor changes (47). Whole blood was collected by standard phlebotomy techniques via venipuncture in 3.2% sodium citrate vacutainers (4.5 mL, BD, Franklin Lakes, NJ). First, the blood was carefully layered over 3 mL of lympholyte poly separation media (Cedarlane Labs, Burlington, Ontario, Canada) and centrifuged at 500*g* for 50 min at 25°C. Second, the neutrophil layer was then removed, diluted to 10 mL with Hank's balanced salt solution without calcium chloride (HBSS, Invitrogen, Grand Island, NY), and spun down at 200*g* for 5 min. Finally, the supernatant was removed and the pellet resuspended in HBSS with 2.4% human serum albumin (HSA, Sigma). For neutrophils receiving drug treatment, cytochalasin D (Sigma) suspended in DMSO was added to a final concentration of 10 μM and incubated for 10 min at 37°C. For the mixed cell experiment, in addition to the neutrophil isolation, 4 μL of whole blood was washed in HBSS and centrifuged at 200*g* for 5 min. The unswollen RBCs were then re-suspended in HBSS/HSA buffer before being added to the isolated neutrophils.

Microfluidic Device Preparation

Microfluidic devices were fabricated in PDMS (Slygard 184, Dow Corning, Midland, MI) using standard soft lithography techniques (48,49). The resulting devices, with channel cross-sectional area of 20 μm × 200 μm and an overall length of 2.5 cm, were ~1.1 mm thick. This thickness of PDMS allows the aspheric lens to focus the optical stretcher through the PDMS layer into the flow channel (46). To prevent leaking in such thin devices, an additional block of PDMS (0.5 cm × 0.5 cm × 1.5 mm) was bonded over the inlet and exit wells to act as a connector between tubing and the device. Channels were incubated with PBS buffer for RBC experiments or HBSS buffer for neutrophil experiments for 1 h. Cells were then flowed through the device at a free-stream cell velocity of ~2000 μm/s, achieved by varying the hydrostatic head 5 ± 2 cm. Initially, free-stream velocity was measured in the absence of optical forces by manually tracking cell position in flow. We define an applied optical intensity in units of mW/μm as the power of the laser is distributed along the length of the 1 μm × 100 μm source. With this, optical intensity was 26.3 mW/μm for the RBC experiments and 40.9 mW/μm for neutrophil and mixed-cell experiments. Exposure for each cell type and condition can be determined by multiplying the optical intensity by the cell cross-section within the trap. With cells spending ~0.01 s in the trap while flowing, they experience a total energy exposure of ~2.0 mJ; low enough to prevent cell damage (50,51).

Image Processing

All videos were captured using the Phantom Camera Control software (Vision Research) at 1,000 fps. Dynamic cell relaxation was processed using a custom C program with functions from the OpenCV computer vision library (52). Briefly, in each frame imaging noise was first removed by cvSmooth before applying an adaptive threshold with cvAdaptiveThreshold. Cell contours were then detected with cvFind-Contours and fit to ellipses using cvFitEllipse2. The ellipse fit chooses the major and minor axes diameters and centroid position. Using size and position information, cell trajectories were tracked and used to store raw data for individual cells. The image analysis and data processing codes are available on GitHub (https://github.com/marrgroup/imageanalysiscode).

Cell data across the region of interest (125 μm × 15 μm), illustrated in Figure 2a as a dotted rectangle, were separated further into two regions (solid boxes in Fig. 2a): maximum cell deformation at the end of the optical stretcher and cell relaxation 30 μm downstream of the stretcher. The time available and the hydrodynamic forces in the system limit any cell rotation in this distance after the optical stretcher. The average cell size parameters in these boxed regions were used to calculate deformation parameters including percent deformation of the major axis, $(A - A0)/A_0$, percent deformation of the minor axis, $(B - B_0)/B_0$, stretched aspect ratio, $D = (A/B)$, and relaxed aspect ratio, $D_0 = (A_0/B_0)$, where A and B represent the stretched major and minor cell diameters, and A_0 and B_0 represent the relaxed cell diameters. Scatter plots for data visualization were generated with a custom Matlab function, *dscatter*, available on the Mathworks File Exchange (File ID: #8430).

Flow Cytometry

To measure the relative concentration of cells in our mixed population, we performed cytometry analysis with a Guava easyCyte Single Sample Flow Cytometer (EMD Millipore, Billerica, MA). Isolated neutrophils were stained in a 5 μM solution of DiOC6 (Sigma) for identification. RBCs were then mixed with the neutrophils as described above for the mixed cell samples and run in the cytometer. Gating was determined based on fluorescence and confirmed with pure neutrophils.

Statistical Analysis

Statistical significance between groups was determined by two-sample *t*-tests in Matlab. A P value of less than 0.01 was considered significant. Data was plotted on a log–log scale to more readily differentiate between small differences in population deformation.

Results and Discussion

Microfluidic devices were designed to create a hydrodynamic focusing flow profile (53) (Fig. 2a). Cells in suspension were guided to the linear optical stretcher by focusing the center inlet with two buffer streams. The stretcher has a steep intensity gradient along the short beam axis allowing cells to be tightly held in that direction. The long beam axis lacks the same steep gradient, allowing cells to freely travel along the stretcher long axis as they are driven down the channel by flow. Upon entering the stretcher, cells experience an optical force at the membrane surface from a change in momentum of refracted laser light (Fig. 2b). The magnitude of the resulting force is strongly dependent on the angle of the incoming light, described by the focusing NA. For a linear optical trap where the width is shorter but the length is longer than a cell diameter, we have previously demonstrated that an NA of ~0.5 will generate the maximum stretching force (37). The anisotropic intensity distribution creates antipodal stretching forces and cell elongation along the long beam axis (Fig. 2b) (37). Here, the beam is aligned with flow, allowing cells to stretch (Fig. 2c) as they translate along the long axis of the stretcher. After cells exit the stretcher they relax back to their pre-stretched state. To quantify this, the camera is positioned to observe both the point of maximum deformation at the end of the stretcher and the cell relaxation down the channel, shown as a dotted region in Figure 2a. RBCs were fully relaxed 30 μm downstream of the end of the trap. However, the technique does not require full relaxation to determine differences because only relative differences are used to discriminate cell state or type.

Untreated, diamide-treated, and glutaraldehyde-treated RBCs were measured at throughputs averaging 15.0 ± 10.0 cells/s, with a range of 5–50 cells/s (Fig. 3) at an optical intensity of 26.3 mW/μm. Considering an average cell spacing of 20 μm to ensure accurate image processing, the theoretical maximum measurement throughput for a flow rate of 2,000 μm/s is ~100 cells/s. Rigid colloids were employed as a control for image processing as they do not deform under applied optical force and used to generate the solid line in the aspect ratio plots corresponding to zero deformation (Supporting Information Fig. 1a). We present our data in Figure 3 as stretched (D) vs. unstretched (D_0) aspect ratios where data further from the origin denote increasing cell asymmetry and data above the line greater cell deformability. Normal RBCs (Fig. 3a) deform 6.5 ± 6.0% with respect to the major axis (Fig. 3d). RBCs treated with diamide (Fig. 3b) deform an average of 3.9 ± 8.5% (Fig. 3d). Diamide causes disulfide bonds to form between membrane spectrin proteins resulting in a stiffening of the cell membrane (54–56). RBCs treated with glutaraldehyde (Fig. 3c) remained undeformed, on average, by the same optical force (Fig. 3d) due to the non-specific crosslinking of membrane proteins by glutaraldehyde (57–59). Note that despite the spread in cell morphology distribution (e.g. Fig. 3a), measured deformations are consistent as indicated by the data falling parallel to the line, an observation verified by plotting the major axis percent deformation directly (Supporting Information Figs. 1b and 1d).

Deformation of normal and cytochalasin D-treated neutrophils was measured at an average throughput of 3.0 cells/s, limited by the concentration of the isolated neutrophil suspension. Normal neutrophils (Fig. 4a) were measured to have an average of $D = 1.15 \pm 0.16$ (Fig. 4c), with 86% of the population found in the region bounded by $\ln(D)$ and $\ln(D_0) < 0.3$. Neutrophils treated with cytochalasin D experience cell softening (60,61) via disruption in cytoskeletal Factin (62,63). Such softening is observed in the upward shift of the cytochalasin D-treated neutrophils (Fig. 4b) to $D = 1.21 \pm 0.18$ (Fig. 4c). Neutrophils have a reported cortical tension (26.8 μN/m (63)) three- to fourfold stiffer than the shear elastic modulus of RBCs (6–9 μN/m (64,65)) and thus require a larger optical power (40.9 mW/μm) to induce measurable deformation. Although the average percent deformation of the neutrophil major axis (~1%) is low at this increased optical intensity, it is sufficient to differentiate between behavior of normal and treated cells.

RBC and neutrophils were mixed in a suspension at relative concentrations of 48.7% and 51.3%, respectively, as determined using a fluorescent marker for neutrophils in a flow cytometer (Fig. 5a), and stretched at an optical power of 40.9 mW/μm and measurement throughput of 3 cells/s. Two gating styles were applied to discriminate the two cell types by aspect ratio. Figure 5b shows a scatter plot of deformation data with gating criteria extracted from the untreated pure cell population plots. The neutrophils in the mixed population are found in the same location as the untreated neutrophils in Figure 4a bounded by $\ln(D)$ and $\ln(D_0) < 0.3$. RBCs are found above this region in the area of $\ln(D)$ and $\ln(D_0) > 0.3$ and above the rigid colloid line. In Figure 3a, 77% of the RBCs are found in this region. Although the RBCs in Figure 3 were deformed at a lower optical power (26.3 mW/μm) than in the mixed cell experiment (40.9 mW/μm), it is reasonable that the vast majority of the RBCs deformed at the higher power will fall in or above this same region. In the mixed cell experiment, 88.0% of the cells in the mixed population are positively identified in either of the two gating regions, of which 43% are identified as neutrophils (815) and 57% are identified as RBCs (1,080). We also gated samples based on cell size, using a cell diameter of 5.5 μm for discriminating RBC and neutrophils (Fig. 5b). The larger cells, corresponding to the neutrophils, comprised 46% of the cell population with the remaining 54% identified as the smaller RBCs; percentages consistent with identification based on deformability as well as measured by flow cytometry. The slight drop in measured neutrophils in the aspect ratio measurements is likely due to neutrophil adhesion at the device inlet leading to a decrease in concentration.

In this study, we used a linear optical stretcher to measure deformation response by applying a non-contact force on flowing blood cells. This approach is capable of distinguishing differences in cell populations, either by chemical treatments that affect the mechanical properties of the plasma membrane or cytoskeleton or in mixtures of RBC and neutrophils. The ability to apply optical forces decoupled from cell size is unique, as size is directly coupled to applied force via flow rate in other high-throughput methods (28,29). By separating deforming force from flow rate, one can fix hydrodynamic conditions while varying the applied force, allowing direct comparison between cell types of different stiffness and size at the same velocity. As the optical train is independent of the characterization optics (46), the optics could be potentially integrated with existing imaging cytometery platforms (66) utilizing existing image capture and processing software (66) to quantify cell deformation.

Supplementary Material

Refer to Web version on PubMed Central for supplementary material.

Acknowledgment

The authors would like to thank Kuldeepsinh Rana, Joanna Slyman, and Aditya Kasukurti for helpful discussions.

Grant sponsor: National Institute of Allergy and Infectious Disease

Grant sponsor: National Institutes of Health; Grant number: 1R01AI079347

Literature Cited

1. Suresh S. Biomechanics and biophysics of cancer cells. Acta Mater 2007;55:3989–4014.
2. Hoffman BD, Crocker JC. Cell mechanics: Dissecting the physical responses of cells to force. Annu Rev Biomed Eng 2009;11:259–288. [PubMed: 19400709]
3. Lee GYH, Lim CT. Biomechanics approaches to studying human diseases. Trends Biotechnol 2007;25:111–118. [PubMed: 17257698]
4. Nash G, Brien O, Gordon-Smith E, Dormandy EJ. Abnormalities in the mechanical properties of red blood cells caused by *Plasmodium falciparum*. Blood 1989;74:855–861. [PubMed: 2665857]
5. Stuart J, Nash G. Red cell deformability and haematological disorders. Blood Rev 1990;4:141–147. [PubMed: 2245249]
6. Baskurt O Deformability of red blood cells from different species studied by resistive pulse shape analysis technique. Biorheology 1996;33:169–179. [PubMed: 8679963]

7. Guck J, Schinkinger S, Lincoln B, Wottawah F, Ebert S, Romeyke M, Lenz D, Erickson HM, Ananthakrishnan R, Mitchell D. Optical deformability as an inherent cell marker for testing malignant transformation and metastatic competence. Biophys J 2005;88:3689–3698. [PubMed: 15722433]
8. Li QS, Lee GYH, Ong CN, Lim CT. AFM indentation study of breast cancer cells. Biochem Biophys Res Commun 2008;374:609–613. [PubMed: 18656442]
9. Remmerbach TW, Wottawah F, Dietrich J, Lincoln B, Wittekind C, Guck J. Oral cancer diagnosis by mechanical phenotyping. Cancer Res 2009;69:1728–1732. [PubMed: 19223529]
10. Jordan MA, Wilson L. Microtubules and actin filaments: Dynamic targets for cancer chemotherapy. Curr Opin Cell Biol 1998;10:123–130. [PubMed: 9484604]
11. Zhou J, Giannakakou P. Targeting microtubules for cancer chemotherapy. Curr Med Chem Anticancer Agents 2005;5:65–71. [PubMed: 15720262]
12. Di Carlo D A mechanical biomarker of cell state in medicine. J Lab Autom 2012;17: 32–42. [PubMed: 22357606]
13. Lam WA, Rosenbluth MJ, Fletcher DA. Chemotherapy exposure increases leukemia cell stiffness. Blood 2007;109:3505–3508. [PubMed: 17179225]
14. Fletcher DA, Mullins RD. Cell mechanics and the cytoskeleton. Nature 2010;463: 485–492. [PubMed: 20110992]
15. Evans EA, Waugh R, Melnik L. Elastic area compressibility modulus of red cell membrane. Biophys J 1976;16:585–595. [PubMed: 1276386]
16. Schmid-Schonbein G, Sung K, Tozeren H, Skalak R, Chien S. Passive mechanical properties of human leukocytes. Biophys J 1981;36:243–256. [PubMed: 6793106]
17. Weisenhorn AL, Khorsandi M, Kasas S, Gotzos V, Butt HJ. Deformation and height anomaly of soft surfaces studied with an AFM. Nanotechnology 1993;4:106–113.
18. Henon S, Lenormand G, Richert A, Gallet F. A new determination of the shear modulus of the human erythrocyte membrane using optical tweezers. Biophys J 1999;76: 1145–1151. [PubMed: 9916046]
19. Dao M, Lim C, Suresh S. Mechanics of the human red blood cell deformed by optical tweezers. J Mech Phys Solids 2003;51:2259–2280.
20. Guck J, Chilvers ER. Mechanics meets medicine. Sci Transl Med 2013;5:212fs41.
21. Di Carlo D, Lee LP. Dynamic single-cell analysis for quantitative biology. Anal Chem 2006;78:7918–7925. [PubMed: 17186633]
22. Cho SH, Chen CH, Tsai FS, Godin JM, Lo Y-H. Human mammalian cell sorting using a highly integrated micro-fabricated fluorescence-activated cell sorter (μFACS). Lab Chip 2010;10:1567. [PubMed: 20379604]
23. Ishii S, Tago K, Senoo K. Single-cell analysis and isolation for microbiology and biotechnology: Methods and applications. Appl Microbiol Biotechnol 2010;86:1281–1292. [PubMed: 20309540]
24. Whitesides GM. The origins and the future of microfluidics. Nature 2006;442:368–373. [PubMed: 16871203]
25. Rosenbluth MJ, Lam WA, Fletcher DA. Analyzing cell mechanics in hematologic diseases with microfluidic biophysical flow cytometry. Lab Chip 2008;8:1062–1070. [PubMed: 18584080]
26. Bow H, Pivkin IV, Diez-Silva M, Goldfless SJ, Dao M, Niles JC, Suresh S, Han J. A microfabricated deformability-based flow cytometer with application to malaria. Lab Chip 2011;11:1065. [PubMed: 21293801]
27. Byun S, Son S, Amodei D, Cermak N, Shaw J, Kang JH, Hecht VC, Winslow MM, Jacks T, Mallick P, et al. Characterizing deformability and surface friction of cancer cells. Proc Natl Acad Sci USA 2013;110:7580–7585. [PubMed: 23610435]
28. Otto O, Rosendahl P, Mietke A, Golfier S, Herold C, Klaue D, Girardo S, Pagliara S, Ekpenyong A, Jacobi A, et al. Real-time deformability cytometry: On-the-fly cell mechanical phenotyping. Nat Methods 2015;12:199–202. [PubMed: 25643151]
29. Gossett DR, Tse HTK, Lee SA, Ying Y, Lindgren AG, Yang OO, Rao J, Clark AT, Di Carlo D. Hydrodynamic stretching of single cells for large population mechanical phenotyping. Proc Natl Acad Sci USA 2012;109:7630–7635. [PubMed: 22547795]

30. Dudani JS, Gossett DR, Tse HTK, Di Carlo D. Pinched-flow hydrodynamic stretching of single-cells. Lab Chip 2013;13:3728. [PubMed: 23884381]
31. Tse HTK, Gossett DR, Moon YS, Masaeli M, Sohsman M, Ying Y, Mislick K, Adams RP, Rao J, Di Carlo D. Quantitative diagnosis of malignant pleural effusions by single-cell mechanophenotyping. Sci Transl Med 2013;5:212ra163–212ra163.
32. Lincoln B, Erickson HM, Schinkinger S, Wottawah F, Mitchell D, Ulvick S, Bilby C, Guck J. Deformability-based flow cytometry. Cytometry A 2004;59A:203–209.
33. Ananthakrishnan R, Guck J, Wottawah F, Schinkinger S, Lincoln B, Romeyke M, Moon T, Käs J. Quantifying the contribution of actin networks to the elastic strength of fibroblasts. J Theor Biol 2006;242:502–516. [PubMed: 16720032]
34. Kim D-H, Wong PK, Park J, Levchenko A, Sun Y. Microengineered platforms for cell mechanobiology. Annu Rev Biomed Eng 2009;11:203–233. [PubMed: 19400708]
35. Ashkin A Applications of laser radiation pressure. Science 1980;210:1081–1088. [PubMed: 17831450]
36. Guck J, Ananthakrishnan R, Moon T, Cunningham C, Käs J. Optical deformability of soft biological dielectrics. Phys Rev Lett 2000;84:5451–5454. [PubMed: 10990966]
37. Sawetzki T, Eggleton CD, Marr DWM. Cell elongation via intrinsic antipodal stretching forces. Phys Rev E 2012;86: 061901(5).
38. Neuman KC, Block SM. Optical trapping. Rev Sci Instrum 2004;75:2787. [PubMed: 16878180]
39. Svoboda K, Block SM. Biological applications of optical forces. Annu Rev Biophys Biomol Struct 1994;23:247–285. [PubMed: 7919782]
40. Sraj I, Szatmary AC, Desai SA, Marr DWM, Eggleton CD. Erythrocyte deformation in high-throughput optical stretchers. Phys Rev E 2012;85: 041923(9).
41. Sawetzki T, Eggleton CD, Desai SA, Marr DWM. Viscoelasticity as a biomarker for high-throughput flow cytometry. Biophys J 2013;105:2281–2288. [PubMed: 24268140]
42. Sraj I, Eggleton CD, Jimenez R, Hoover E, Squier J, Chichester J, Marr DWM. Cell deformation cytometry using diode-bar optical stretchers. J Biomed Opt 2010;15: 047010. [PubMed: 20799841]
43. Applegate RW, Squier J, Vestad T, Oakey J, Marr DWM. Optical trapping, manipulation, and sorting of cells and colloids in microfluidic systems with diode laser bars. Opt Express 2004;12:4390–4398. [PubMed: 19483988]
44. Applegate RWJ, Squier J, Vestad T, Oakey J, Marr DWM, Bado P, Dugan MA, Said AA. Microfluidic sorting system based on optical waveguide integration and diode laser bar trapping. Lab Chip 2006;6:422. [PubMed: 16511626]
45. Applegate RW, Squier J, Vestad T, Oakey J, Marr DWM. Fiber-focused diode bar optical trapping for microfluidic flow manipulation. Appl Phys Lett 2008;92:013904.
46. Roth KB, Neeves KB, Squier J, Marr DWM. Imaging of a linear diode bar for an optical cell stretcher. Biomed Opt Express 2015;6:807. [PubMed: 25798305]
47. Oh H, Siano B, Diamond S. Neutrophil isolation protocol. J Vis Exp 2008; e745 [DOI: 10.3791/745].
48. Duffy D, McDonald J, Schueller O, Whitesides G. Rapid prototyping of microfluidic systems in poly(dimethylsiloxane). Anal Chem 1998;70:4974–4984. [PubMed: 21644679]
49. Sia SK, Whitesides GM. Microfluidic devices fabricated in Poly(dimethylsiloxane) for biological studies. Electrophoresis 2003;24:3563–3576. [PubMed: 14613181]
50. Ashkin A, Dziedzic J, Yamane T. Optical trapping and manipulation of single cells using infrared laser beams. Nature 1987;330:769–771. [PubMed: 3320757]
51. Roth KB, Eggleton CD, Neeves KB, Marr DWM. Measuring cell mechanics by optical alignment compression cytometry. Lab Chip 2013;13:1571–1577. [PubMed: 23440063]
52. Bradski G, Kaehler A. Learning OpenCV: Computer Vision with the OpenCV Library, 1st ed. Sebastopol, CA: O'Reilly Media; 2008.
53. Knight J, Vishwanath A, Brody J, Austin R. Hydrodynamic focusing on a silicon chip: Mixing nanoliters in microseconds. Phys Rev Lett 1998;80:3863–3866.

54. Fischer TM, Haest CW, Stöhr M, Kamp D, Deuticke B. Selective alteration of erythrocyte deformabiliby by SH-reagents: Evidence for an involvement of spectrin in membrane shear elasticity. Biochim Biophys Acta 1978;510:270–282. [PubMed: 667045]
55. Chien S Red cell deformability and its relevance to blood flow. Annu Rev Physiol 1987;49:177–192. [PubMed: 3551796]
56. Forsyth AM, Wan J, Ristenpart WD, Stone HA. The dynamic behavior of chemically “stiffened” red blood cells in microchannel flows. Microvasc Res 2010;80:37–43. [PubMed: 20303993]
57. Morel FM, Baker RF, Wayland H. Quantitation of human red blood cell fixation by glutaraldehyde. J. Cell Biol 1971;48:91–100. [PubMed: 5545112]
58. Noji S, Taniguchi S, Kon H. An EPR study on erythrocyte deformability. Prog Biophys Mol Biol 1991;55:85–105. [PubMed: 1651527]
59. Szwarocka A, Jozwiak Z. The effect of daunorubicin and glutaraldehyde treatment on the structure of erythrocyte membrane. Int J Pharm 1999;181:117–123. [PubMed: 10370208]
60. Ting-Beall HP, Lee AS, Hochmuth RM. Effect of cytochalasin D on the mechanical properties and morphology of passive human neutrophils. Ann Biomed Eng 1995; 23:666–671. [PubMed: 7503466]
61. Roca-Cusachs P, Almendros I, Sunyer R, Gavara N, Farré R, Navajas D. Rheology of passive and adhesion-activated neutrophils probed by atomic force microscopy. Biophys J 2006;91:3508–3518. [PubMed: 16891365]
62. MacLean-Fletcher S, Pollard TD. Mechanism of action of cytochalasin B on actin. Cell 1980;20:329–341. [PubMed: 6893016]
63. Tsai MA, Frank RS, Waugh RE. Passive mechanical behavior of human neutrophils: Effect of cytochalasin B. Biophys J 1994;66:2166–2172. [PubMed: 8075350]
64. Hochmuth RM, Waugh RE. Erythrocyte membrane elasticity and viscosity. Annu Rev Physiol 1987;49:209–219. [PubMed: 3551799]
65. Hochmuth RM. Micropipette aspiration of living cells. J Biomech 2000;33:15–22. [PubMed: 10609514]
66. Basiji DA, Ortyn WE, Liang L, Venkatachalam V, Morrissey P. Cellular image analysis and imaging by flow cytometry. Clin Lab Med 2007;27:653–670, viii. [PubMed: 17658411]

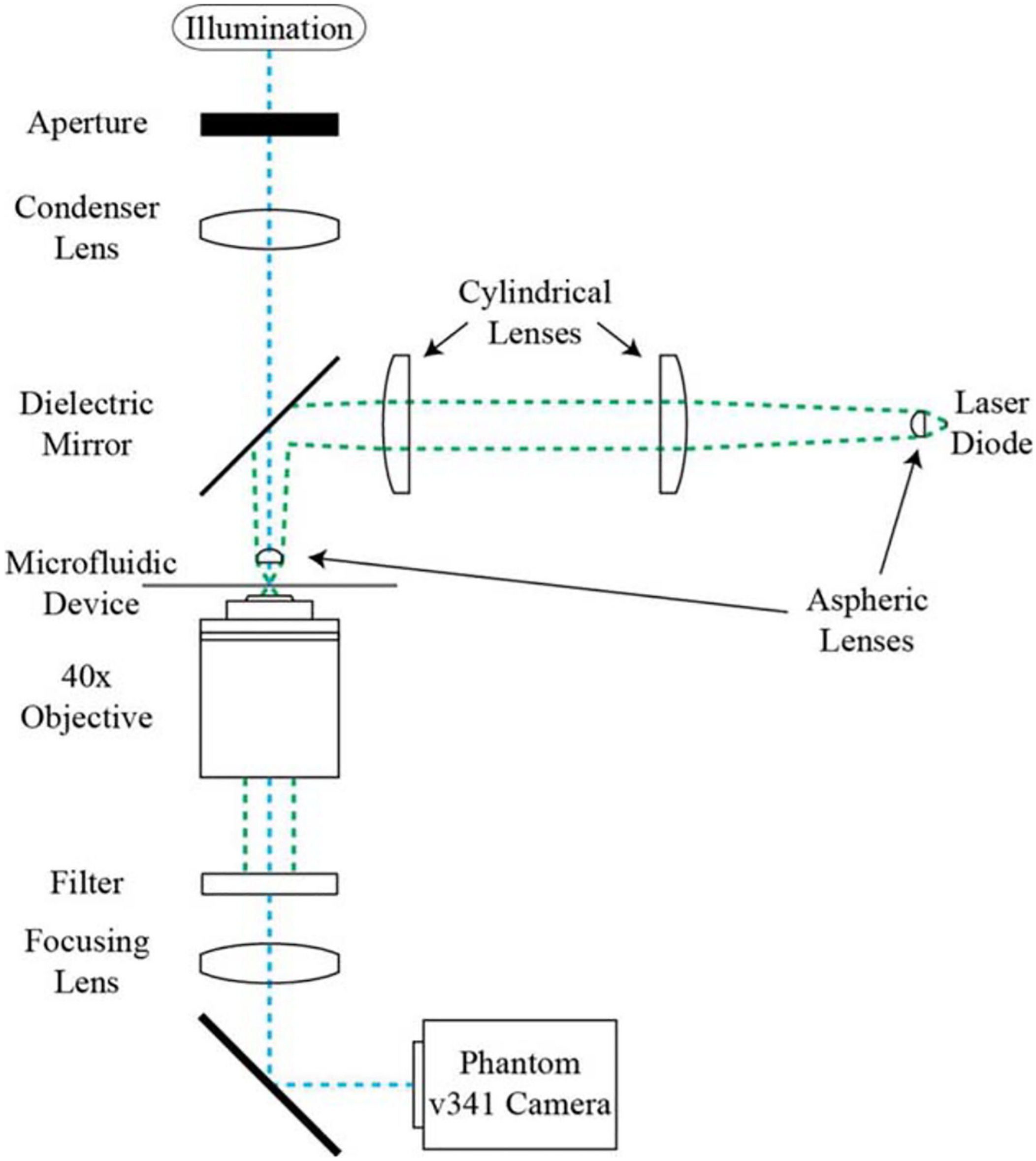

Figure 1.

Linear stretcher optical assembly. A 1:1 image of the laser diode source is formed at the focal plane of a 40× objective. An aspheric lens collimates the laser output, a cylindrical lens telescope corrects for the source geometry, and an identical aspheric lens refocuses the laser. The sample is illuminated from above and an image is formed below on the camera.

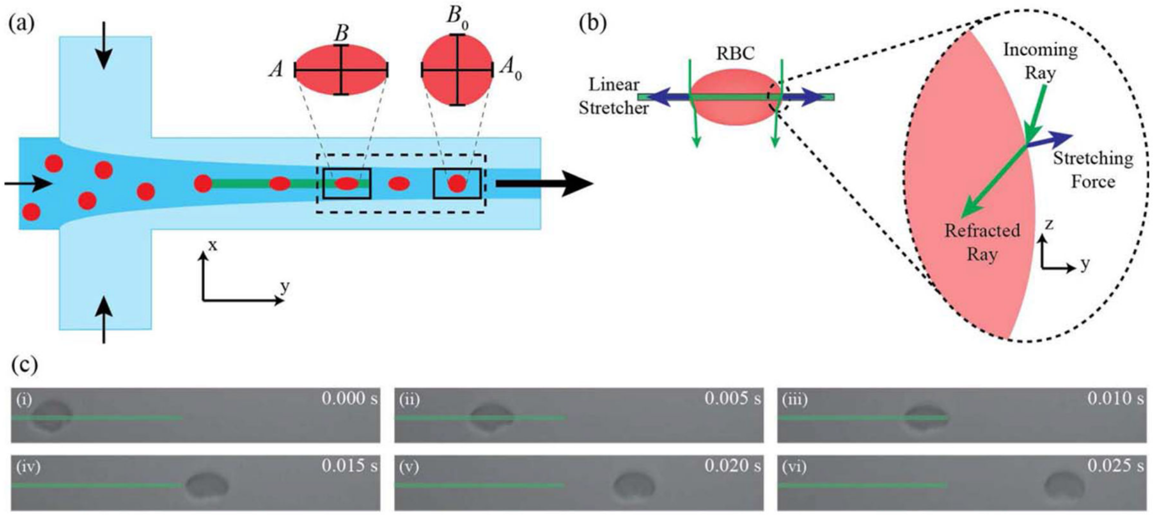

Figure 2.

(**a**) Hydrodynamic focusing device design: Cells enter the focusing region and are guided toward the optical stretcher. Cells are then observed in the rectangular region of interest (125 μm × 15 μm) from stretched to a relaxed state in flow. The solid boxes illustrate the regions of cell stretch and relaxation used to calculate deformation parameters corresponding to the panels of a RBC stretching in flow. (**b**) Optical stretching forces: As an incoming ray of light is refracted at the cell surface, the resulting change in momentum imparts a force on the cell membrane. The resulting net optical force acts to stretch the cell along the line of the trap (37). (**c**) A typical RBC stretch and relaxation cycle. The green bar shows the position of the linear optical stretcher.

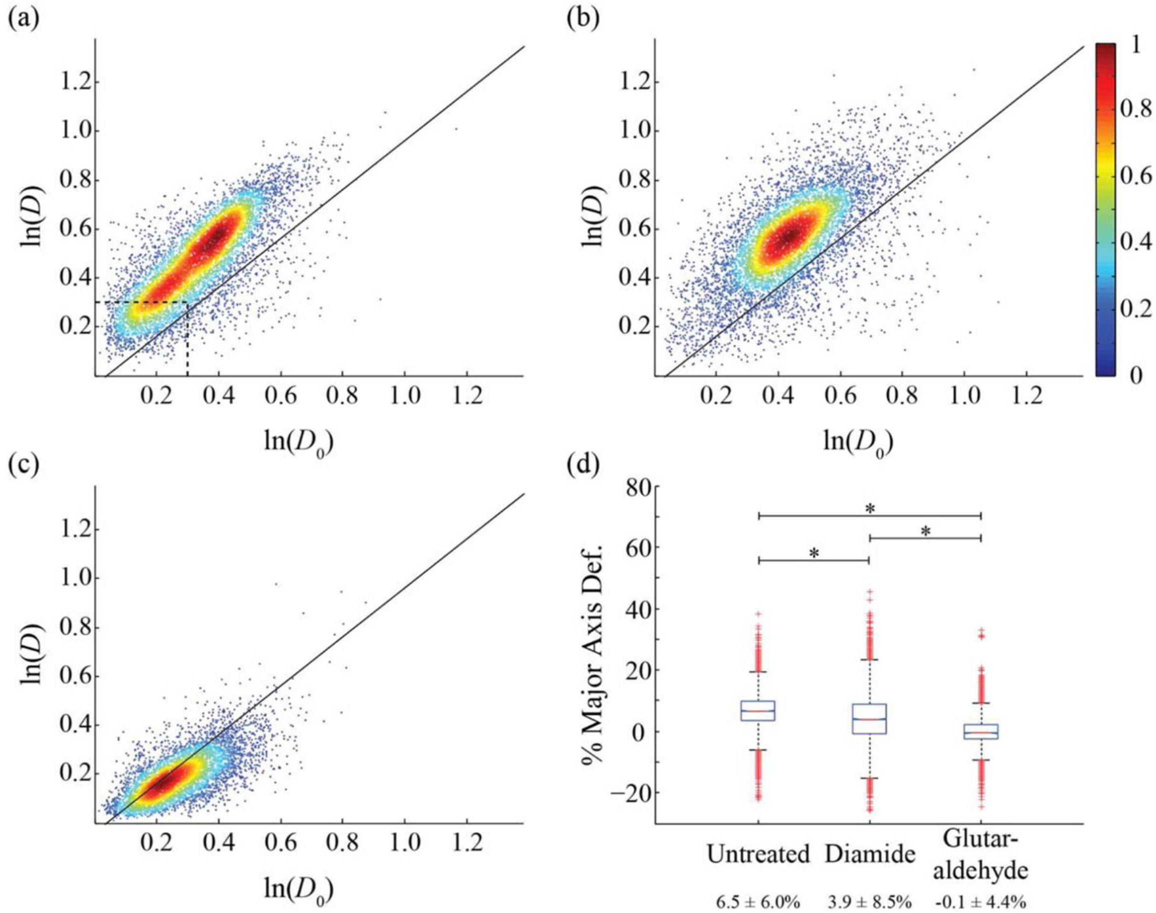

Figure 3.

Cell aspect ratio for pure RBCs. D corresponds to the ratio of the cell's major and minor axis diameters at the end of the optical stretcher, D_0 represents the same ratio 30 μm down the flow channel. (**a**) Untreated (n = 8,098), (**b**) treated with 3.8 mM diamide (n = 7,917), (**c**) treated with 0.05% vol/vol glutaraldehyde (n = 5,883). Solid lines correspond to measurements on rigid colloids. (**d**) Box plot of the average percent deformation of the major axis with average values and standard deviations from data in panels (a–c). (*) corresponds to a P values of 10^{-4} for a two-sample t test. The color bar shows a scale for the normalized population density. The dashed line in (a) identifies the location of the neutrophil population in Figure 4a.

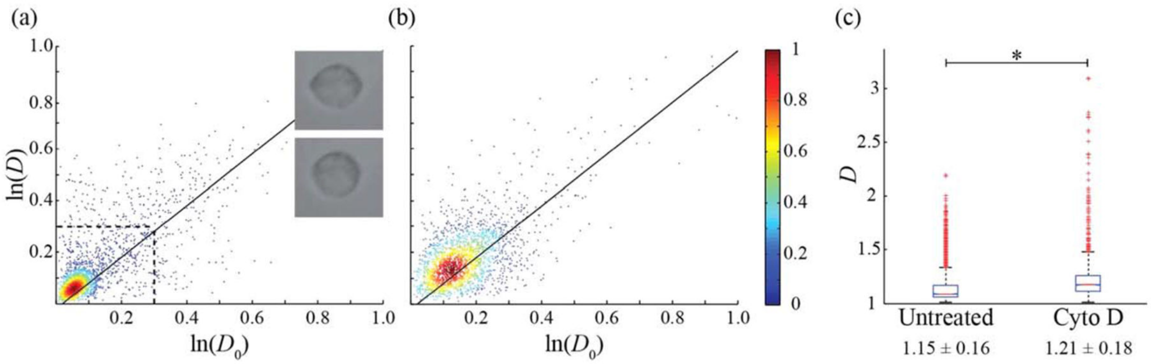

Figure 4.

Cell aspect ratio for neutrophils. (**a**) Untreated (n = 2,389), (**b**) Cytochalasin D treated (n = 2,199). Solid lines correspond to measurements on rigid colloids. (**c**) Box plot of D with average values and standard deviations for data in panels (a) and (b). (*) corresponds to a P values of 10^{-4} for a two-sample t test. The dashed line in (a) corresponds to the region containing 86% of the total neutrophil population with images of a stretched (top) and relaxed neutrophil (bottom) provided for clarification.

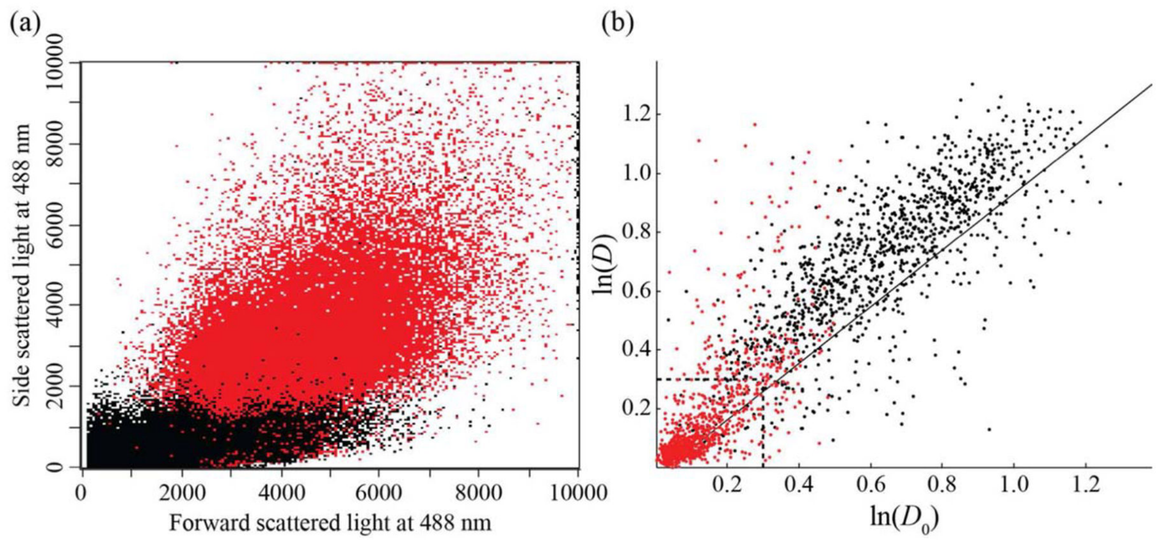

Figure 5.

RBC and neutrophil mixed population. (**a**) Flow cytometry data of forward and side scatter for a mixed cell population (n = 113,981), with neutrophils shown in red and RBCs in black. Neutrophil gating was based on the fluorescence of a pure population of neutrophils. Neutrophils (red) comprise 51.3% of the population (mean fluorescence intensity of 1,146.09 with 88.10% CV), while RBCs (black) comprise the balance (mean fluorescence intensity of 3.41 with 302.14% CV). (**b**) Mixed cell population (n = 2,154) gated by size. The red population corresponds to minor axis diameters above 5.5 µm (n = 993), the black population corresponds to minor axis diameters below 5.5 µm (n = 1,161).